Coastal High Frequency Radar Wind Turbine Interference Mitigation

U.S. Department of the Interior
Bureau of Ocean Energy Management
Office of Renewable Energy Programs
Sterling, Virginia

BOEM
Bureau of Ocean Energy
Management

Coastal High Frequency Radar Wind Turbine Interference Mitigation

December, 2021

Authors:
Dale Trockel, Josh Trockel, Chad Whelan

Prepared under 140M0120C0002

By
CODAR Ocean Sensors Ltd.
1914 Plymouth Street,
Mountain View, California 94043

BOEM
Bureau of Ocean Energy
Management

DISCLAIMER

Study concept, oversight, and funding were provided by the U.S. Department of the Interior, Bureau of Ocean Energy Management (BOEM), Environmental Studies Program, Washington, DC, under Contract Number140M0120C0002. This report has been technically reviewed by BOEM, and it has been approved for publication. The views and conclusions contained in this document are those of the authors and should not be interpreted as representing the opinions or policies of BOEM, nor does mention of trade names or commercial products constitute endorsement or recommendation for use.

REPORT AVAILABILITY

To download a PDF file of this report, go to the U.S. Department of the Interior, Bureau of Ocean Energy Management Data and Information Systems webpage (http://www.boem.gov/Environmental-Studies-EnvData/), click on the link for the Environmental Studies Program Information System (ESPIS), and search on 2021-081. The report is also available at the National Technical Reports Library at https://ntrl.ntis.gov/NTRL/.

CITATION

Trockel D., Trockel J., Whelan C. 2021. Coastal High Frequency Radar Wind Turbine Interference Mitigation. Sterling, VA: U.S. Department of the Interior, Bureau of Ocean Energy Management. 37 p. Report No.: OCS Study BOEM 2021-081. Contract No.: 140M0120C0002.

ACKNOWLEDGMENTS

Contents

List of Figures

List of Tables

List of Abbreviations and Acronyms

BLCK	Block Island
BOEM	Bureau of Ocean Energy Management
CCL	Compact Cross Loop
CFAR	Constant False Alarm Rate
CODAR	Coastal Ocean Dynamics Application Radar
FFT	Fast Fourier Transform
FMCW	Frequency-Modulated Continuous-Wave
HF	High Frequency
HFR	High Frequency Radar
IOOS	NOAA's Integrated Ocean Observing System
NEC	Numerical Electromagnetic Code
NOAA	National Oceanic and Atmospheric Administration
RCS	Radar Cross Section
RPM	Rotations Per Minute
SCADA	Supervisory Control and Data Acquisition
SNR	Signal to Noise Ratio
WTI	Wind Turbine Interference
2D	two dimensional

1 Introduction

Coastal high frequency radars (HFR) are the only instruments capable of making both high spatial and temporal resolution measurements of sea surface currents over large observation areas. In the U.S., a network of HFR stations maintained in partnership with the U.S. Integrated Ocean Observing System (IOOS) monitors ocean currents across much of the outer continental shelf in U.S. Waters. The observations from the U.S. HFR network are assimilated in the Coast Guard's search and rescue models, improving reliability, and narrowing search areas for people and vessels lost at sea (H. Roarty et al.). Similarly, the sea surface current measurements help focus oil spill cleanup efforts (Abascal et al., 2017). More recently, the National Weather Service has begun assessing HFR wave measurements for wave forecasting. Other applications of the national network include tsunami detection (outputs of which are transmitted to NOAA's Tsunami Warning Center) (Lipa et al., 2016), wind measurements (Kirincich, 2016), and vessel detection (H. J. Roarty et al.), among others. NOAA's U.S. IOOS Office spends approximately $7,000,000 per year on HF Radar operations and maintenance and coverage expansion. Additionally, the historical record of data collected from the HFR network spans several decades, making it an invaluable resource to researchers.

The presence of offshore wind turbines is known to impact radar systems. A recent study (Colburn et al., 2020) found that coastal HFR will be the most impacted of all land radar systems due to their prevalence on the coast and their large area of observation. The majority of the coastal HFR are SeaSondes, which are manufactured by CODAR Ocean Sensors Ltd. There are over 140 SeaSondes in operation in the U.S. national network. With the increase in offshore wind energy, mitigation of wind turbine interference (WTI) is essential to maintaining the integrity of the HFR national network. In 2019, a community working group of researchers, radar operators, and radar manufactures authored a white paper with comprehensive recommendations to mitigate WTI impacts on HFR (Kirincich et al., 2019). The Bureau of Ocean Energy Management (BOEM) contracted with CODAR Ocean Sensors Ltd. to develop a WTI simulation tool and a real-time WTI mitigation software solution completing recommendations 1–3 in the community white paper. The purpose of this report is to describe the work done to complete these tasks.

As early as 2011, researchers found impacts of WTI on HFR ocean observations (Wyatt et al., 2011). Teague and Barrick (2012) identified the amplitude modulation of the periodic radar cross-section (RCS) of a rotating wind turbine as the cause of the WTI. The amplitude modulation of the RCS results in different WTI impacts on HFR than experienced on other radar systems. Due to the difference in the WTI, the mitigation techniques developed for other radar technologies are not applicable. Trockel et al. (2018) derived the functional relationship between the rotation rate of the turbine blade and the location of the WTI in the range-Doppler spectrum and identified the impacts of the WTI on SeaSonde radars. Trockel et al. (2018) also proposed the first WTI mitigation algorithms for HFR. Several mitigation techniques were tested and it was found that methods that solve both a forward and inverse problem were most effective. This method used radar data to estimate the rotation rates of the turbines (the inverse problem) and then used the estimated rotation rates to approximate the WTI signal that was mixed with the radar data. Mitigation testing was done using simulations of a single turbine and the five-turbine Block Island Wind Farm impacting 5 and 25 MHz SeaSonde compact cross loop (CCL) systems.

The mitigation proposed was computationally expensive and not scalable to a field-ready solution.

The purpose of this work was to develop a scalable simulation tool and WTI mitigation software for SeaSonde HFR. Expanding on the work of Trockel et al. (2018), the capability of the WTI simulation tool was extended to simulate WTI from multiple wind turbines of varying sizes simultaneously. Additionally, many of the shortcomings of the previous mitigation methods were addressed, and those solutions were implemented in a software WTI mitigation package for SeaSonde radars. By integrating the mitigation strategy developed herein, it is estimated that the impact of the WTI at a test SeaSonde site on Block Island is reduced by 86.4%. The remainder of this report is organized with general background in chapter 1, methods of the simulation, mitigation, and testing in chapter 2, results in chapter 3, a discussion of the results and their implications in chapter 4, and we finish with our concluding remarks and recommendations in chapter 5.

1.1 Background

Coastal oceanographic HFR operating at a frequency range of 4–50 MHz are mainly used to measure the current of the ocean near the surface. Their high frequency (HF) signal propagates as a groundwave, following the curvature of the ocean surface beyond the horizon, enabling them to make observations over large areas with high temporal resolution.

Table 1: Operational Parameters for BLCK SeaSonde.

Parameter	Value	Notation
Start Frequency	4.6213 MHz	f_c
Band width	25.734 kHz	B
Sweep Rate	4 Hz	$\dfrac{1}{T}$
Doppler FFT Length	4096	N
Range Bin Size	5.8249 km	
Doppler Bin Size	0.00097656 Hz	

HFRs make surface current observations by transmitting a frequency-modulated continuous-wave (FMCW) with the frequency increasing linearly throughout each sweep, as depicted in Figure 1. The transmitted signal starts at a frequency of f_c at the beginning of each sweep and is increased over a bandwidth of B throughout each sweep to $f_c + B$. The signal is reflected off of ocean waves and other hard targets back to the receiver. The received signal is then mixed with the transmitted signal, and the signal at each range is extracted by applying a short-time fast Fourier transform (FFT) with a Hamming window to each sweep of length T seconds. A second long-time FFT with a Hamming window is applied to the results from N successive sweeps at each range, giving the range-Doppler decomposition. The results of the double FFT processing produce a range-Doppler matrix spectrum as seen in Figure 2. The vertical axis in Figure 2 indicates the range from the radar, and the horizontal axis shows the Doppler frequency for each range bin. The range resolution is given by $\frac{c}{2B}$ and the Doppler resolution is $\frac{c}{2NTf_c}$ where c is the

speed of light. The regions circled in red indicate the portion of the Doppler spectra containing the sea echo, and the red arrows indicate the location of the WTI from the Block Island wind farm. The portion of the range-Doppler spectra containing the sea echo is referred to as the "first-order region" or the "Bragg region" due to the constructive Bragg scattering from the sea surface responsible for the strong signal in this region. An important part of the SeaSonde data processing involves isolating the Bragg region from the remaining range-Doppler spectra and is done using a proprietary constant false alarm rate (CFAR) method using the noise floor estimates at the edges of the Doppler spectra in each range cell.
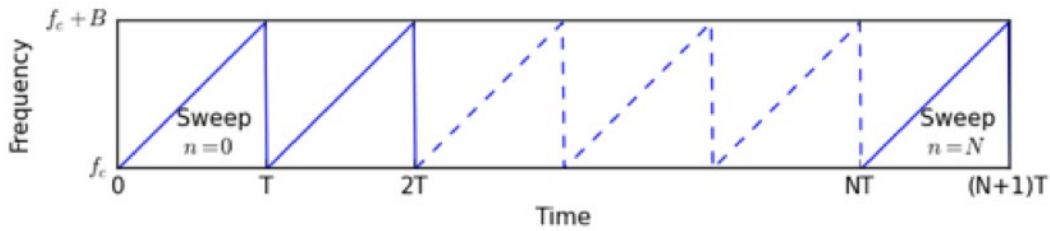
Figure 1: The frequency of the transmitted FMCW waveform for a SeaSonde radar with a sweep repetition period of *T* seconds, start frequency f_c, and bandwidth *B*.

Trockel et al. (2018) identified two ways that WTI degrades SeaSonde ocean observations. First, when the WTI peaks are located within the Bragg region, the bearing determination of the sea surface current observations is compromised. Second, the WTI can obscure the boundary of the first-order region or result in an over-estimation of noise levels on the edges of the Doppler spectra, both problems lead to errors identifying the first-order region.
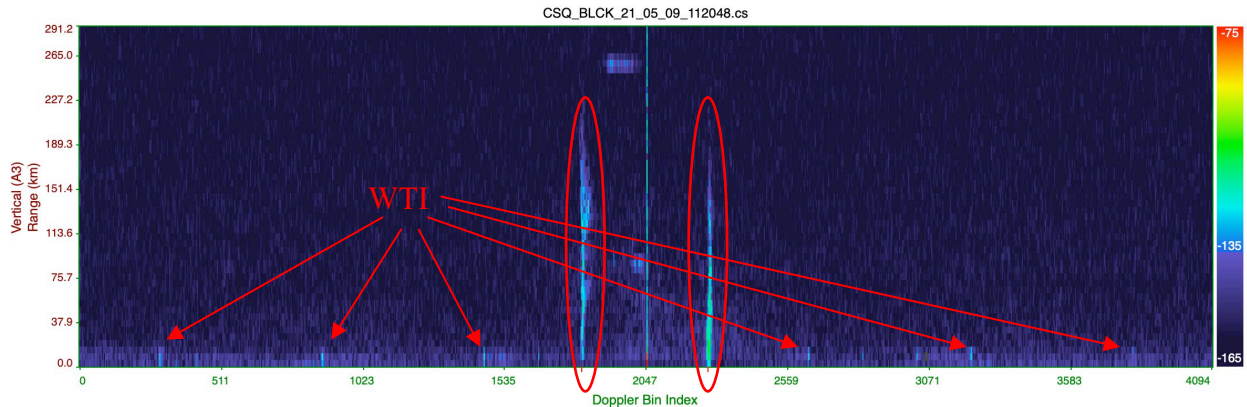
Figure 2: An example range-Doppler spectrum containing WTI collected with a 5 MHz radar at Block Island 5 km from the turbines. The regions circled in red indicate the portion of the Doppler spectra containing the sea echo. The WTI is indicated with the red arrows.

1.2   WTI Characteristics

Teague and Barrick (2012) showed the Doppler shift of the signal reflected by a wind turbine's rotating blades had too low of a signal to noise ratio (SNR) to appear above the noise floor in a

SeaSonde range-Doppler spectra. Rather, the interference observed is caused by the harmonic components of the amplitude modulated signal reflected from the turbines. The periodic amplitude of the HF signal reflected from a wind turbine, $a(t)$, can be represented as the sum of its harmonic components as

$$a(t) = \sum_{m=-\infty}^{\infty} a_m e^{i2\pi mt},$$ (1)

where m is the harmonic number. Each harmonic component gets placed in a different range-Doppler bin. The amplitude and variability in the periodic signal reflected from the turbines, $a(t)$, determines the number of harmonic components with amplitudes, a_m, large enough to interfere with the radar's surface current observations. As the turbines get larger, they reflect more energy and the variability of the $a(t)$ increases. For example, the turbines in the Block Island wind farm have a mast around 102–260 m tall, have a blade length of around 73–107 m, and it was observed that only the first four positive and negative harmonics were above the noise floor. For comparison, the larger Haliade-X 12 MW turbine has a mast length of around 260 m, a blade length of 107 m, and simulations indicate the first nine harmonics will have a large enough amplitude to cause interference. For the simulations used in this work, the turbines at Block Island were modeled using the parameters found in Table 2. The amplitudes of the first twenty positive and negative harmonics for a simulated wind turbine are shown in the plot of Figure 3.

The location of the WTI harmonic peaks in range and Doppler frequency is a function of the rotation rate, r, of a turbine. Trockel et al. (2018) traced the harmonic components of WTI through the dual FFT SeaSonde FMCW processing to derive the range and Doppler frequency of each harmonic. It was shown that for a turbine at distance R_t from the radar with a sweep repetition period of T and a bandwidth of B, the range, R_m, the harmonic component number m will appear at is given by

$$R_m = R_t + \frac{c}{2B}\left[\frac{3Tm}{60} + \frac{1}{2}\right].$$ (2)

The Doppler frequency, f_m, of the mth harmonic was likewise obtained to be

$$f_m = \left[\left(\frac{3mr}{60}\right) mod \frac{1}{T}\right] - \frac{1}{2T}$$ (3)

where the modulus function, mod, accounts for aliasing when the Nyquist frequency is exceeded. An example of the position of the first three positive and negative WTI harmonics is shown in the bottom plot of Figure 3 for the 5 MHz SeaSonde at Block Island with a sweep rate of 4 Hz and the operational turbines rotating at 11.45 RPM.

The goal of the mitigation methods outlined in the following chapters is to identify and flag the WTI in the Doppler spectra. The flagged range-Doppler cells can then be omitted from the algorithm used to find the first-order region and process sea surface current measurements. Equations (2) and (3) are fundamental for the mitigation methods outlined below as they show the precise location of the WTI in the SeaSonde's range-Doppler spectra once the rotation rates are known.
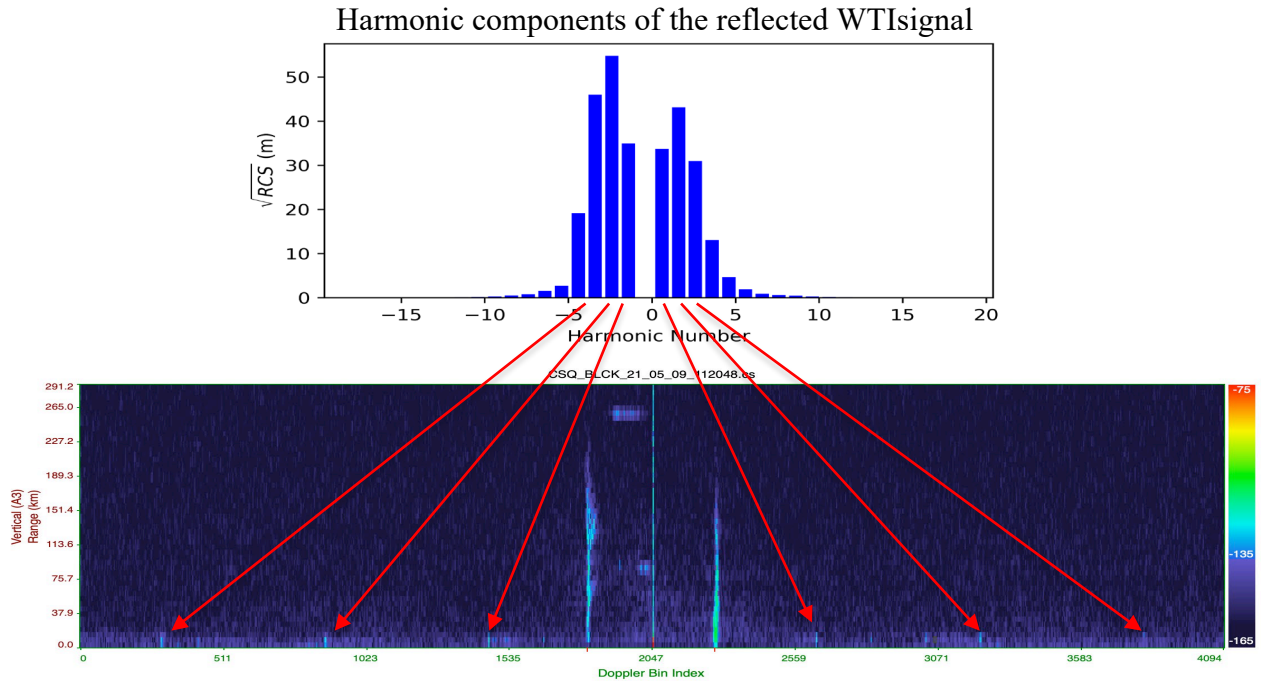
Figure 3: The harmonic components of the signal reflected from a wind turbine at Block Island (top) and their observed locations in the range-Doppler spectra of a 5 MHz SeaSonde 5 km away. Only the first three positive and negative harmonics have a high enough SNR to be detectable.

2 Method

This section describes the methods used by CODAR to simulate and mitigate WTI impact on coastal HFR. Working with BOEM, CODAR collected data from the 5 MHz radar at Block Island along with rotation rates and yaw angles to calibrate the developed simulation and mitigation tools. Additionally, the mitigation assessments and data sets used to test the mitigation methods are reviewed at the end of this chapter.

2.1 Simulation

Currently, there are only two offshore wind farms in the United States. Because of the limited number of offshore wind turbines in U.S. waters, and no known instances outside the U.S. with offshore wind turbines in the field of view of any HFR, it is not possible to investigate the impacts of WTI or the effectiveness of WTI mitigation methods without the use of WTI simulations. CODAR extended the Numerical Electromagnetics Code (NEC) WTI simulation previously developed by Trockel et al. (2018) to allow the impact assessment of large wind farms in diverse configurations. The improvements include the ability to model multiple turbines of different sizes rotating at different rates. The simulated signals from multiple turbines are combined and processed using CODAR's dual FFT FMCW processing to estimate the range-Doppler spectral components of the WTI from an offshore wind farm. The simulated WTI is then scaled and added to a SeaSonde Doppler spectra to show what the interference would be like if the wind farm were in the observational area of the SeaSonde.

For the description of the simulations below, we consider only a single turbine. Since the range-Doppler processing is linear, the signal from multiple turbines can be added together at the end of the processing to simulate the WTI from multiple turbines.

2.1.1   Simulating the Reflected WTI Voltage Signal

Since the transmitted wave lengths from a HFR are large, the Doppler shift of the reflection of a wind turbine's rotating blades has too low a signal-to-noise ratio (SNR) to impact the SeaSonde data processing. However, at different yaw angles and different rotation angles of the turbine's fan, the turbine's RCS—a measure of the reflectivity of an object— changes. Due to the trifold symmetry of the turbine's blades, for a fixed yaw angle, the RCS of the turbine is a periodic function with a period of 120° of rotation. The periodic RCS of the wind turbine creates a periodic amplitude-modulated reflected signal. An example of the RCS of a rotating turbine is shown in Figure 4. The signal reflected for a turbine will be proportional to the RCS of the turbine.
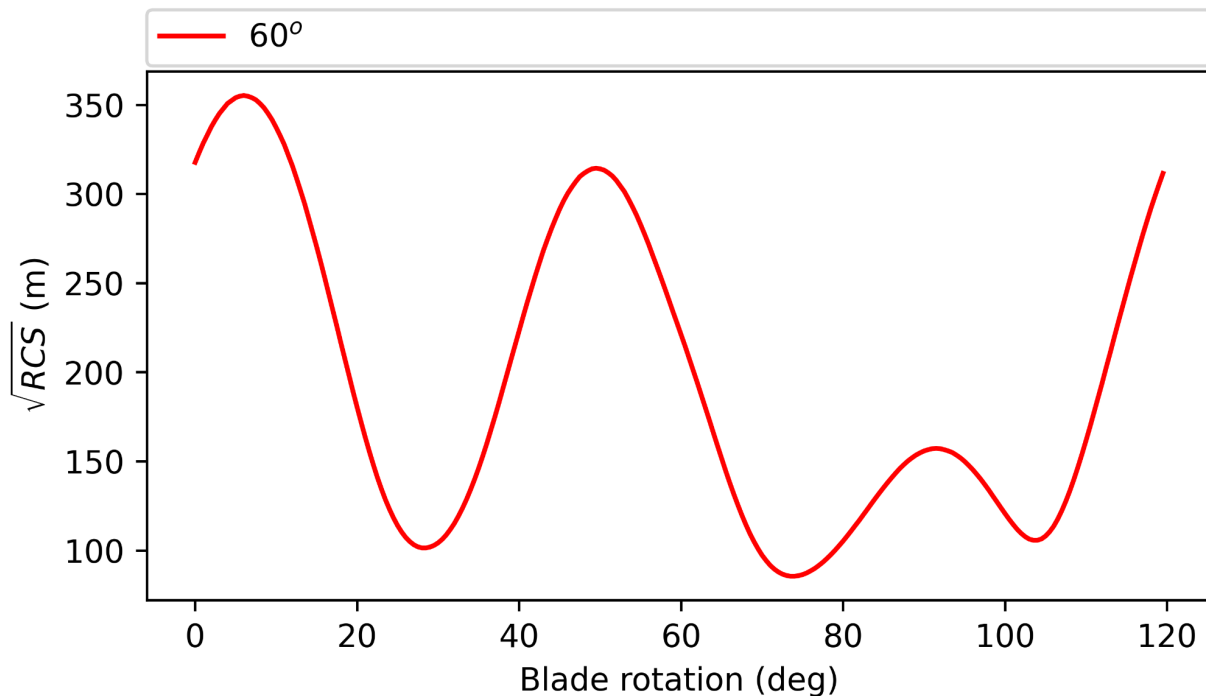
Figure 4: An example of the RCS of a turbine as its fan rotates 120° with a fixed yaw angle of 60° relative to the radar. The periodic RCS of a wind turbine results in an amplitude modulated reflection.

CODAR simulated the reflected signal of the wind turbine echo using NEC following the methods outlined in (Trockel, et al. 2018) and (Teague and Barrick 2012), which we will give a brief review of here. In the first steps, the WTI from each of the turbines is determined separately and then combined to get the WTI from the entire wind farm. To get the voltage time-series, NEC was used to simulate the RCS of each wind turbine with the fan in different positions. The turbine was represented as a wireframe model as shown in Figure 5. Several simulations were run with the fan rotated 0° to 120° in one-degree increments and yaw angles ranging from 0° to

90°. With three identical blades, the RCS values repeat precisely after rotating 120°. Using prespecified rotation rates of each of the turbines, a time series of rotation angles was made to align with the sample times of the radar. Quadratic interpolation was used on the RCS output from NEC to get the RCS of each of the turbines at each rotation angle, forming a time series of radar cross-sections. Using $rcs(\theta(t), \phi)$ to represent the NEC estimated RCS of a wind turbine with a fan rotation angle $\theta(t)$ at time t, and fixed yaw angle ϕ, the reflected signal from a wind turbine is given by

$$c_0 \frac{1}{R^2} rcs(\theta(t), \phi) v \left(t - \frac{t_d}{2} \right), \tag{4}$$

where c_0 is a proportionality constant, t_d is the travel time of a radio wave to the turbine and back to the radar, and $v(t)$ is the transmitted voltage signal.
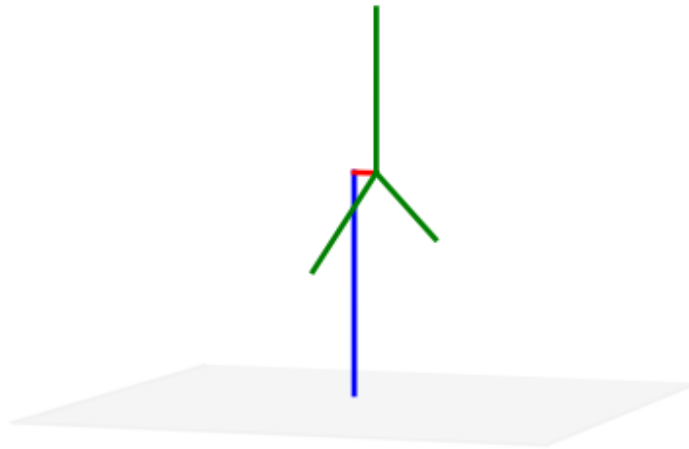
Figure 5: A wireframe representation of a wind turbine used as input to NEC to simulate the RCS of the wind turbine.

To save processing time, during simulations, NEC outputs are stored within a database. If the turbine position, angles, and dimensions do not exist within the database, they will be created and then stored for future use.

Table 2. Parameters used with NEC

Parameter	Value
Mast Height	100 m
Hub Length	10 m
Blade Length	40 m
Number of Blade Segments	20
Number of Mast Segments	50
Number of Hub Segments	2
Frequencies	5 MHz, 13.5 MHz, 25 MHz, 42 MHz
Sweep Bandwidth	25 kHz

In order to facilitate access to the database, as well as enable multiprocessing capabilities, when creating large simulated datasets, a local server was created to house the database and allow easy access through pull requests. This allows the more computationally intensive aspects of the simulation to be parallelized without having to worry about duplication and file handling. The simulation tool developed by CODAR allows the user to provide parameters within configuration files to determine the turbine position, angle, and dimensions necessary for NEC.

2.1.2   Received Voltage Signal to Spectra

Once created, the RCS is scaled and added to a SeaSonde cross spectra file to simulate the effect a turbine, with those given parameters, would have in the field. Further parameters can be specified for the interference scaling, location, and bearing.

2.1.2.1   Range Doppler Processing of WTI

Following the FMCW processing outlined in (Barrick 1973), the RCS time series of a turbine, given in equation (4) above, is multiplied by the transmitted signal from the radar giving the de-chirped signal

$$v_m(t) = c_0 rcs\left(\theta\left(t - \frac{t_d}{2}, \phi\right)\right) v(t - t_d)v(t) \tag{5}$$

A Fast Fourier Transform (FFT) is applied to each radar sweep, yielding the wind turbine interference signal at each range bin for that sweep. FFT outputs from successive sweeps are grouped by range and processed for Doppler frequency using a second FFT. This results in a 2D range-Doppler spectra, which will then be scaled and added to a SeaSonde's range-Doppler spectra. The resulting simulated 2D range-Doppler spectra at range cell i and doppler cell j is represented as s_{ij}. An example of simulated range-Doppler spectra for the turbine parameters in Table 2 is shown in Figure 6. The turbine in Figure 6 was placed 58 km from the radar and had an arbitrary simulated rotation rate of 6.2 RPM. It should be noted that this is not a common rotation rate for turbines of this size.
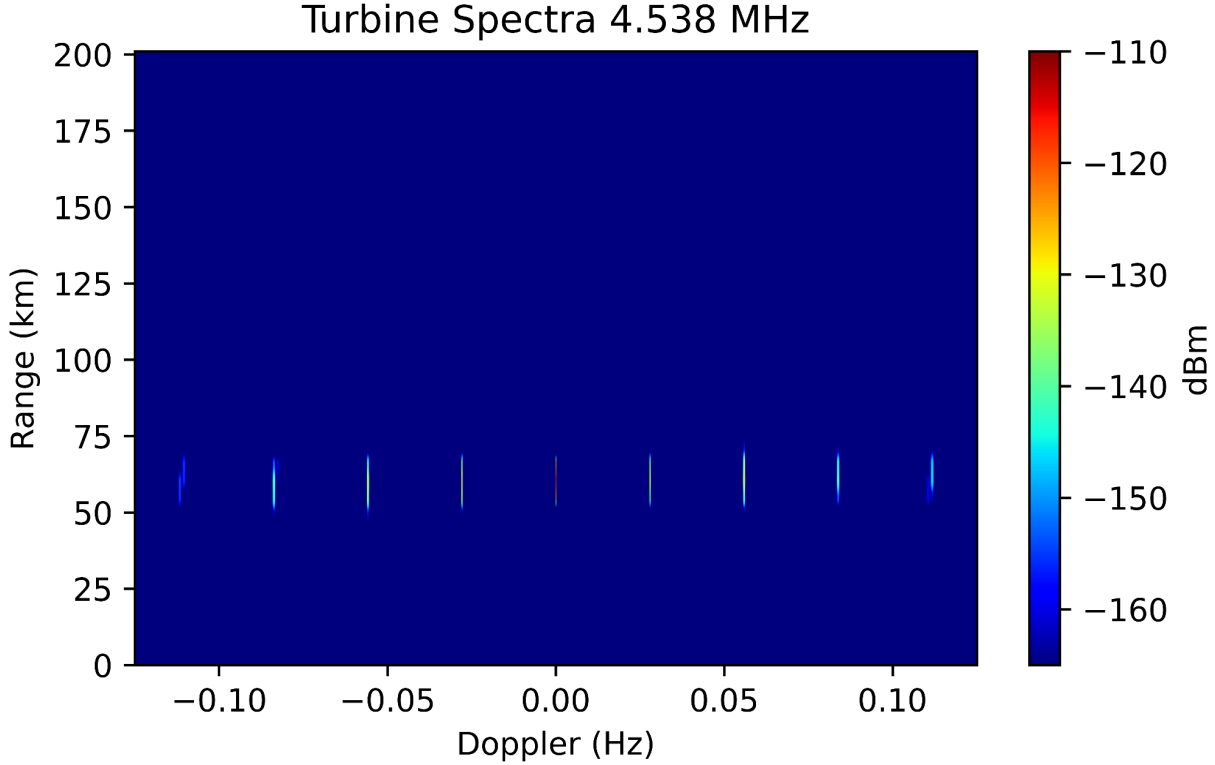
Figure 6: Simulated WTI range-Doppler spectra after scaling has been applied. The simulation was placed 58 km from the radar and had a simulated rotation rate of 6.2 RPM.

2.1.2.2 Bearing Assignment

SeaSondes use three co-located perpendicular antennas: a vertical monopole, and two horizontal cross loop antennas. The antenna response pattern measured at the SeaSonde site is used to simulate the response of the three antennas to the angle of arrival. The simulated signal on each antenna was obtained by multiplying equation (5) by the antenna response at that azimuth. The simulated signals for each of the antennas are combined at each range-Doppler bin to obtain the SeaSonde cross spectra. Using the simulated signal, s_{ij}, at range bin i and Doppler bin i the cross spectra is given by

$$C_{ij} = a(\varphi)s_{ij}s_{ij}^*a^*(\varphi), \tag{6}$$

where $a(\varphi)$ is the measured antenna response vector for azimuth, φ, to the turbine and * represents the complex conjugate. For more details, see (Barrick 1973).

2.1.2.3 Scaling

The simulated WTI is scaled before being added to the cross spectra. The actual scaling of the signal is a function of environmental conditions and the range of the turbine from the radar. However, due to the complexity of resolving the changing environmental conditions, the relative strength of the WTI to the Bragg signal was used to calculate the scaling coefficients. The scaling is specified within the configuration file and is specified in dB relative to the sea echo.

14

With limited real-world data, it is hard to project the dB strength of the interference. As more wind farms arise, this parameter can be specified to what research shows is realistic for the size/distance/yaw angle of the turbine as well as given the environmental conditions around the turbine and SeaSonde. In this investigation, the scaling factor was left as a user set parameter in the configuration file. This dB entry represents dB relative to the Bragg region of the spectra being processed. For example, an input of -20 dB would scale the WTI so the amplitude of the largest harmonic peak, v_{nec}, is 20 dB below the maximal peak, v_{max}, in the Bragg region of the SeaSonde range-Doppler spectra. With the user-supplied difference in signal strength, d, the scaling constant in equation (5) is given by

$$c_0 = \frac{v_{max}10^d}{v_{nec}}. \tag{7}$$

Figure 7 shows a range slice from the range-Doppler spectra at 58 km after the scaling has been applied.
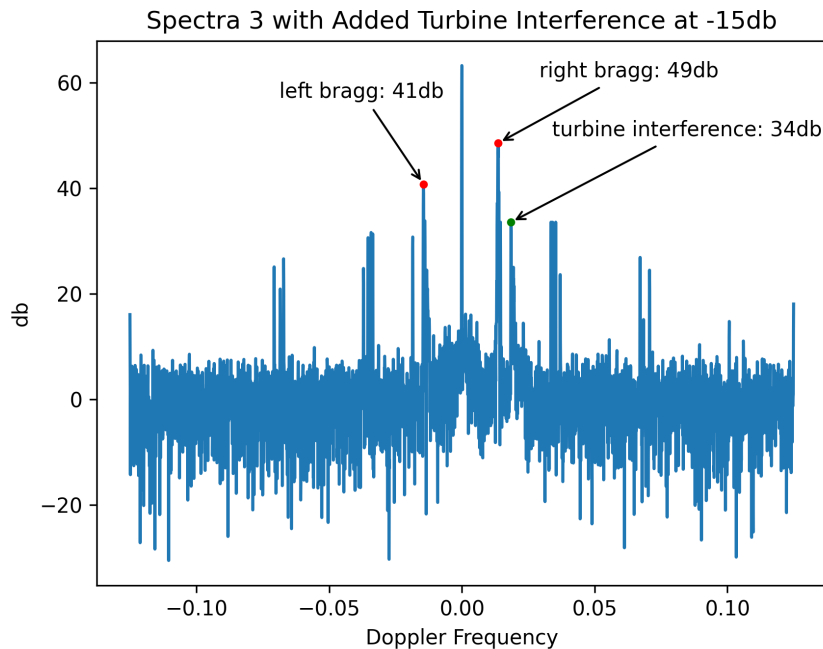
Figure 7: Range slice of a SeaSonde cross spectra with WTI added. Red dots mark the maximal peak of each Bragg region. The green dot marks the maximum simulated WTI harmonic peak scaled to be 15 dB below the max Bragg peak.

2.1.3 Composite signals

To this point, we have focused on generating the signal from a single turbine. In this section, we show the process of combining the signals from each of the turbines to simulate the interference from an entire wind farm. For a set of M turbines, the composite WTI range-Doppler cross spectra is given by

$$C_{ij}^c = \sum_{k=1}^{M} c_0^k C_{ij}^k, \tag{8}$$

where c_0^k is the scaling coefficient of the simulated WTI from turbine k and C_{ij}^k is the covariance matrix of WTI from turbine k at range cell i and Doppler cell j. The composite WTI for four turbines scaled 5 dB down from the Bragg for a turbine 58 km from the radar is shown in Figure 8 along with a SeaSonde range-Doppler spectra before and after the simulated WTI was added. It should be noted that the SeaSonde range-Doppler spectra already has WTI in the first range cell from the Block Island wind farm.
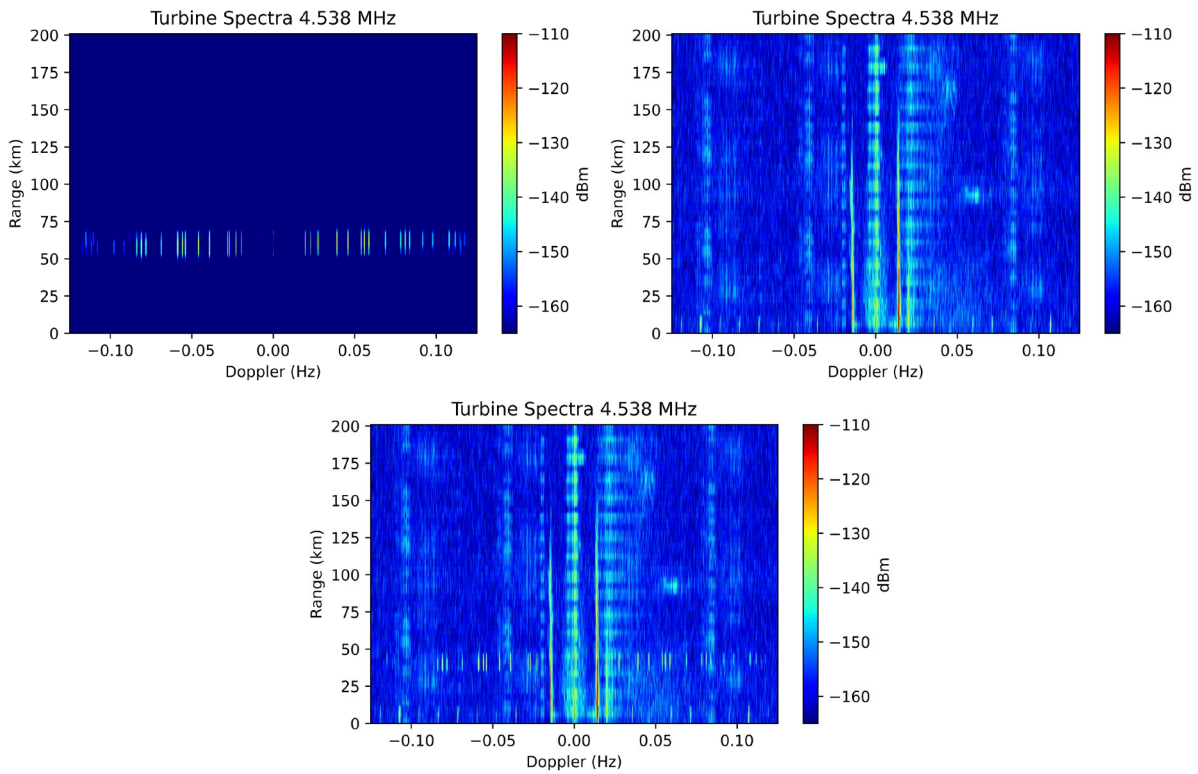
Figure 8: Composite WTI simulated signal for four turbines rotating at 4.9, 4.5, 6.2, 7.1 RPM and respective yaw angles of 18°, 56°, 55°, 69° (left top). Range-Doppler spectra collected from 5 MHz SeaSonde with a 4 Hz sweep rate (right top). SeaSonde range-Doppler spectra with simulated WTI added (bottom).

2.2 Simulations for Mitigation Testing

The simulations used to create a dataset to assess the effectiveness of WTI mitigation are described in this section. Since each range bin is handled independently, the mitigation assessment simulations were all performed by placing a different number of turbines into a single range bin and varying the yaw and rotation rate of each turbine. In the simulation used for this report, the yaw angles and rotation rates were assigned random values, but the specific yaw angles and rotation rates can be specified within the simulation tool if desired. The random rotation rates and yaw angles were used to ensure that the mitigation tool would perform well under diverse conditions. Yaw angles were constrained to 0°– 90°, rotation rate was constrained to 4.5–11.5 RPM.

The bearings are assigned to each of the turbines depending on the number of turbines being simulated. Each turbine is evenly spaced across the coverage indicated in the Measured Pattern. If there are ten turbines and a coverage area of 100°, a turbine would appear every 10°. Thus, each simulated turbine is assigned a bearing based on its location relative to the SeaSonde.

Table 3: Operational parameters of the SeaSonde at Block Island.

Radar Site Code	Center Frequency	Bandwidth	Sweep Rate	Doppler FFT Length
BLCK	4.75 MHz	25.733	4 Hz	4096

The final dataset was simulated using cross spectra from a SeaSonde on Block Island. The operational parameters of the radar can be found in Table 2. The data spanned March 12, 2021 through March 26, 2021. Block Island has a wind farm present, but all interference is found in the first range bin, so simulated interference was placed at a range of 58 km from the SeaSonde, as shown in Figure 8.

The dimensions of the turbines used are shown in Table 1. The testing dataset included six different simulated files for each input SeaSonde spectra file with different scaling constants and the number of turbines. The scales used were 15 dB down from the Bragg, and 0 dB from the max Bragg signal to match the range of scales observed previously for this size of turbine. As more turbines are installed across the coast, these numbers can be varied to account for the size and distance of future wind farms. Exploration into the relationship between size, distance, and yaw angle, and environmental factors and amplitude should be the subject of future investigation. The number of turbines used was 5, 15, and 30. Each combination of scaling and turbines was created for each input SeaSonde spectra file, thus six output files. Each turbine was assigned a random yaw angle (0°–90°) and random rotation rate (4.5–11.5 RPM). The rotation rates had 0 variance added during the Doppler integration period. In total, 7098 files were created.

2.3 Mitigation

With the recent push to expand offshore wind energy in the United States, it is imperative that reliable, robust WTI mitigation be developed for coastal HFR. Without viable mitigation, the data from the U.S. HF radar network will be compromised, impacting end-users such as NOAA and the U.S. Coast Guard. This section describes the mitigation strategies developed by CODAR

under the present contract with BOEM. The mitigation strategies can be split into two categories: mitigation efforts that only require changes to the HFR operating parameters and software implemented mitigations tools that attempt to remove the WTI during the radar's signal processing.

2.3.1 Radar Configuration

The mathematical relationship in equations (2) and (3) show the relationship between the range and Doppler frequency of the WTI harmonic peaks and the sweep rate and wind turbine rotation rate. Examination of equation (3) reveals the importance of the sweep rate in preventing aliasing of the harmonic WTI peaks. Lower sweep periods allow faster rotation rates before aliasing occurs. To illustrate this, the location of the first four positive and negative WTI harmonic peaks are plotted in Figure 9 for rotation rates ranging from 0 to 11.5 RPM for a 5 MHz SeaSonde.

The top plot in Figure 9 shows the harmonic peak locations when the sweep period is set to 1 second. As the rotation rate increases from 0 to around 2.5 RPM, the harmonic peaks increase in Doppler frequency. Once the peaks reach the edge of the Doppler window, they exceed the Nyquist frequency and are aliased around to the other side of the Doppler window where they continue through at the same slope as the rotation rate continues to increase. For illustration purposes, the 4th harmonic position is displayed in blue to highlight the aliasing. The grayed rectangular region in the background of the plots in Figure 9 shows the Doppler frequencies likely to contain the sea echo (i.e., the Bragg region). Notice that due to the aliasing, each peak can pass through the Bragg region multiple times as the rotation rate is increased.

In contrast, the bottom plot of Figure 9 shows the location of the WTI harmonic peaks when the radar sweep rate is set to 4 Hz. With the shorter sweep period only 4th and -4th harmonics are aliased and even then, no harmonic peak passes through the Bragg region more than once. Since there are fewer times the harmonic peaks pass through the Bragg, there are also fewer rotation rates where the WTI will be mixed with the sea echo.
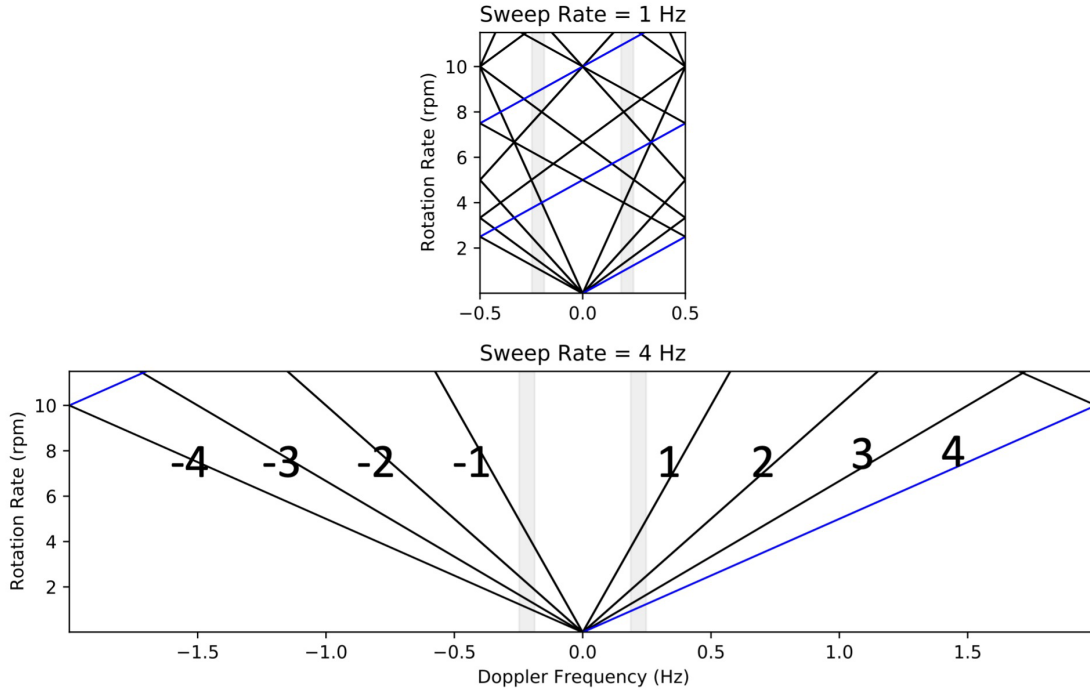
Figure 9: Doppler frequency of WTI harmonic peaks for different turbine rotation rates in 5 MHz SeaSonde cross spectra. The top plot shows the impacts of aliasing at slower 1 Hz sweep rates causing the harmonic WTI peaks to pass through the typical frequencies containing the sea echo multiple times. The bottom plot shows the locations of the WTI harmonic peaks with a sweep rate of 4 Hz, reducing the rotation rates mixing the WTI with the oceanographic data.

To arrive at the optimal sweep rate, several factors must be considered including: the number of observable WTI peaks above the noise floor, the viable rotation rates of the turbine, and the maximum possible sweep rate of the radar. If m_{max} and r_{max} are the maximum observable WTI harmonic peak in the radar's spectra and the maximum turbine rotation rate, then using equation (3) the max sweep period T_{max} before aliasing occurs is given by

$$T_{max} < \frac{10}{m_{max} r_{max}}.$$ (9)

For the 5 MHz SeaSonde at Block Island, the maximal visible WTI harmonic peak is the 4th and the maximum rotation rate of the turbines in the Block Island is 11.5 RPM. Thus, to prevent aliasing the sweep period needs to be less than 0.21 seconds. However, due to software limitations in the SeaSonde, the radar does not perform optimally for sweep periods less than 0.25 seconds or rather a sweep rate of 4 Hz. Furthermore, a sweep rate of 4 Hz is sufficient to prevent aliasing harmonic peaks back into the Bragg regions; CODAR recommends using a sweep rate of 4 Hz.

Before discussing the software mitigation solutions, it should be noted that if the Doppler FFT is done over the same number, N, of sweeps, the Doppler resolution will be decreased. In order to preserve the same Doppler resolution, the time integration period of the FFT must remain the

same. For example, if the sweep rate is increased by a factor of four from 1 Hz to 4 Hz, as recommended, the Doppler FFT length must also be increased by a factor of four.

Increasing the sweep rate also increases the size of the cross spectra files. This can be shown using the 5 MHz Block Island radar (BLCK). Originally, BLCK used a sweep period of 1 second and 1024 sweep Doppler FFT. To reduce aliasing, the sweep rate was set to 4 Hz and the Doppler FFT needed to be increased to 4096 sweeps to maintain the Doppler resolution. This quadrupled the size of the range-Doppler cross spectra files to increase from around 2.4 MB to 9.4 MB. To prevent the need to increase the data storage capacity at radar sites, CODAR developed a tool to clip the added data at the edges of range-Doppler spectra. Removing the edges of the spectra has no impact on ocean observation as it contains no oceanographic data. An example of the spectra before and after the application of the clipping tool is shown in Figure 10.
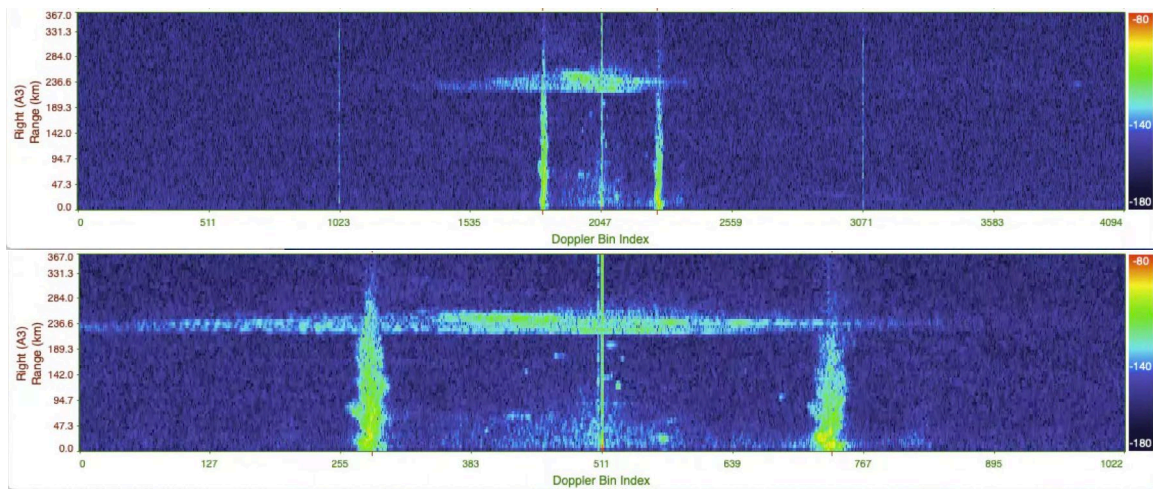
Figure 10: Range-Doppler spectra at the Block Island test site running with a sweep rate of 4 Hz and a Doppler FFT length of 4096. The top image shows the cross spectra before being cropped. The bottom image shows the spectra after being cropped by the cropping software.

2.3.2   Software Mitigation

While tuning the radar can reduce the WTI, it cannot eliminate all of it. To reduce the impact of the WTI further, signal processing methods must be utilized. Trockel et al. (2018) found the most effective mitigation methods was to use a forward and inverse solver. First the rotation rate is estimated from the observable WTI peak in the range-Doppler spectra (the inverse problem). Then the estimated rotation rates are used with equations (2) and (3) to flag all the range and Doppler locations likely containing WTI (the forward problem). A diagram of the process is shown in Figure 11.

Inverse: Estimate Rotation rates   Forward: Flag Doppler locations with WTI

Estimated 11.45 RPM
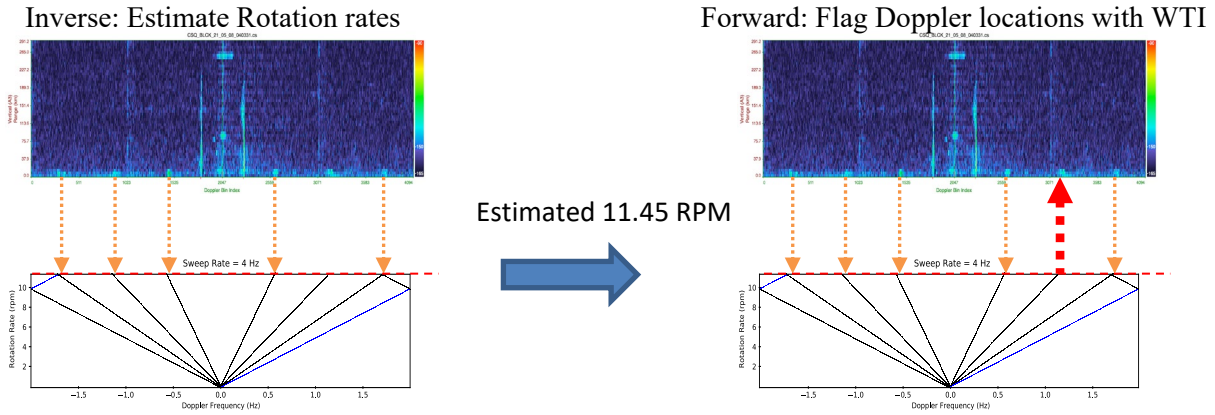
Figure 11: Forward-inverse method to flag range-Doppler bins in SeaSonde spectra that contain WTI. The easily observable WTI peaks are used to estimate the rotation rates of the turbines, then the rotation rates are used to find and flag the remaining WTI peaks not observed.

2.3.2.1 Inverse Method

Trockel et al. (2018) derived the functional relationship between the rotation rate of a wind turbine and the range-Doppler location of the resulting WTI harmonic peaks. However, in most cases, the rotation rates are not known *a priori*. This leads to the need to invert equation (3) to obtain the rotation rates from observable WTI peaks. However, since the harmonic number of each observable WTI peak is unknown, equation (3) does not have a unique inverse.

The method CODAR found to adequately estimate rotation rate from SeaSonde range-Doppler spectra is split into the following steps:

- The possible WTI peaks are identified in the cross spectra.
- The identified peaks and their possible harmonic numbers are used with the inverse of equation (3) to get the set of possible rotation rates.
- The plausible rotation rates are filtered to obtain the final set of estimated rotation rates.

2.3.2.2 WTI Peak Finding

In practice, identifying the WTI peaks is a nontrivial problem. The interference from a single turbine has an identifiable structure in isolation and when the rotation rate is stable. However, when observed by the radar, it is mixed with the sea clutter, other forms of interference, interference from other wind turbines, and the rotation rates are not always stable. Thus, to identify the WTI, peaks that have a similar structure to WTI must be identified while filtering out other forms of interference.

Two structures of wind turbine interference are used to distinguish it from other forms of interference. Namely symmetry and spread in range. By examining equation (3) one will see that, in the absence of aliasing, the positive and negative harmonic interference peaks appear in symmetric locations about zero Doppler. Furthermore, while variation in rotation rate can cause smearing in Doppler, the peaks from a single turbine are isolated to two or three range bins depending on the choice of window used with the Doppler FFT.

Using a narrow spread in range, we can iterate over range cells containing wind turbines and use the symmetric property of the WTI to identify the harmonic peaks as follows:

- Calculate the SNR of the range cell containing the turbines,
- Smooth the range cell to eliminate high frequency variation,
- Threshold the range cell based on the SNR,
- Apply a symmetric threshold operator, and
- Find peaks in the resulting signal.

The following paragraphs explain each step in further detail.

The SNR of range cell i is calculated using the noise floor of the range cell, nf_i. The noise floor is calculated as the median of the values at the edge of the range cell; see the shaded blue area in the range slice displayed in Figure 12. Once the noise floor is obtained, the SNR of each Doppler cell, j, in the range cell in dB is calculated as

$$snr_{ij} = 10 \log\left(\frac{C_{ij}^3}{nf_i}\right), \tag{10}$$

where C_{ij}^3 is the value of the antenna 3 self-spectra at range cell i and Doppler cell j.

Once the srn_{ij} has been calculated, it is smoothed using a moving window average of 20 Doppler bins. The smoothed signal has a threshold applied with a threshold specified in a configuration file. A threshold of 8 dB was used for all tests as that is a typical threshold used for finding hard targets, such as vessels, in SeaSonde data. All Doppler cells with a value of srn_{ij} lower than the specified threshold are set to 0 dB.

To utilize the symmetry of the WTI, the next step is to apply a symmetry operator to the smoothed range cell with applied threshold, snr_{ij}^{thresh}. This is done by setting to 0 dB any point whose symmetric point about zero Doppler is 0 dB. Mathematically this operation is expressed as

$$snr_{ij}^{sym,thresh} = \begin{cases} 0 & if\ snr_{ij*}^{thresh}, \\ snr_{ij}^{thresh} & otherwise \end{cases} \tag{11}$$

where j^* is the symmetric Doppler bin to j relative to the center of the range cell. An example of the resulting $snr_{ij}^{sym,thresh}$ obtained from the range cell containing WTI from the BLCK radar is shown in Figure 13.
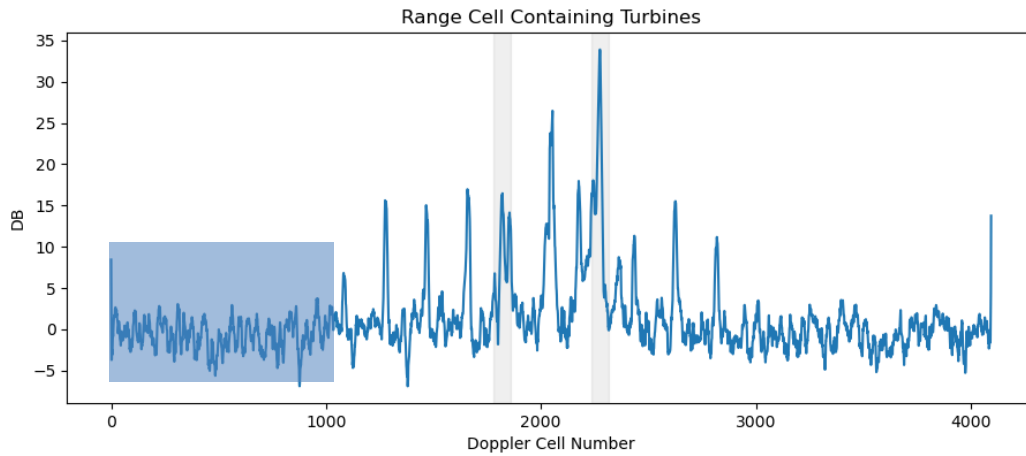
Figure 12: Range cell slice containing WTI. The regions with the gray background indicate the first-order regions. The shaded blue area indicates the region of the spectra used to calculate the noise floor.

The final step is to locate the local maximum of $snr_{ij}^{sym,thresh}$ and collect information on the peak widths. Once potential peaks are located, information including the width of the peak, SNR, height, and a flag indicating if the peak is in the Bragg region is saved for further filtering.
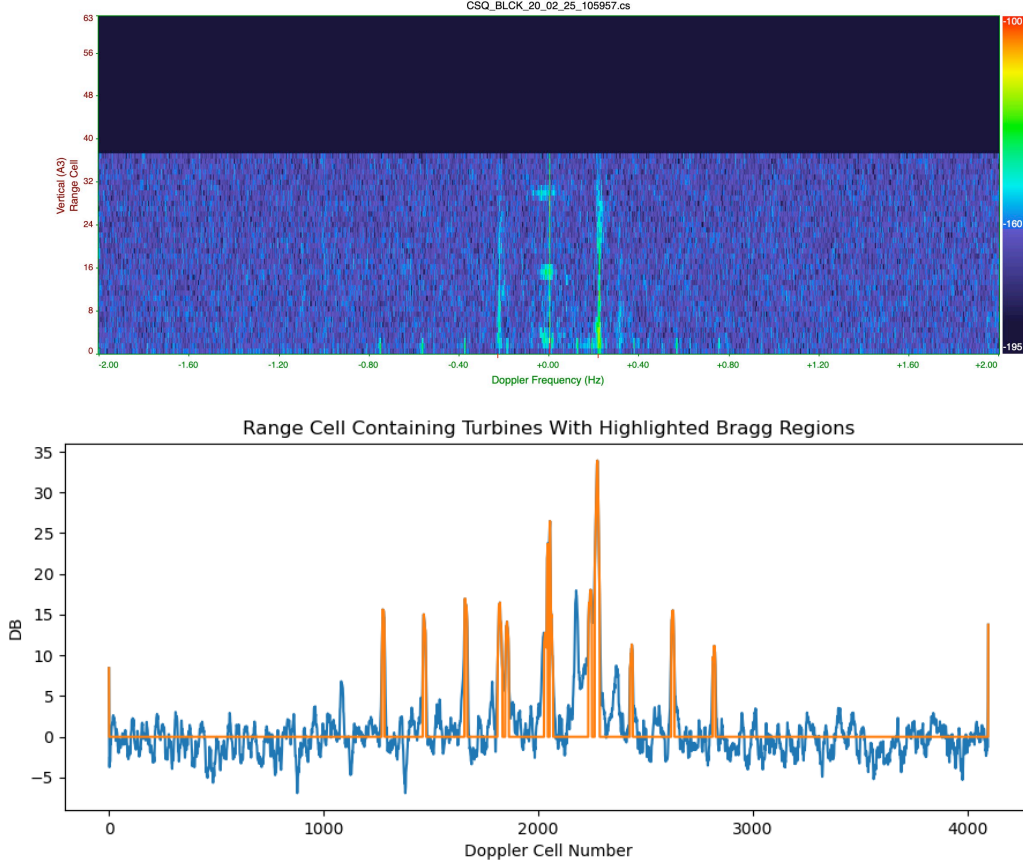
Figure 13: A range-Doppler spectra from BLCK with observed wind turbine interference in the first range cell (top). A range slice of the first range cell in the range-Doppler spectra (bottom). The blue line indicates the SNR of the range cell. The orange line shows the results of applying smoothing, a 10 dB threshold, and symmetric filter.

2.3.2.3 Rotation Rate Estimation

Once all the possible WTI interference peaks have been identified, they are used to form a set of plausible rotation rates. Since the peaks come in symmetric pairs from the previous step, they are processed in pairs. The peak pairs are ordered so that the pairs closest to the center of the range cell are processed first and the ones furthest from the center are processed last. The pairs are then iterated over, applying the inverse of equation (3) to get possible rotation rates.

If the sweep rate has been increased sufficiently to prevent aliasing, the inverse of equation (3) is given by

$$r = \frac{20}{m}\left(f_m - \frac{S}{2}\right), \tag{12}$$

where, as before, $S = 1/T$ is the sweep rate, r is the rotation rate, m is the harmonic component number, and f_m is the Doppler frequency of the peak. Since the true value of m is not known, and multiple WTI harmonic peaks are expected for each rotation rate, the set of possible rotation rates is built iteratively using the most likely values of m. Starting with the harmonic peak pair

closest to the center of the range cell and working outward, the set, Ω, of possible rotation rates and their observed peak, is updated as follows:

- Cycle through all possible values of m (i.e., m=1,…, m_{max}) and estimate the rotation rate using equation (12) to get a set of possible rotation rates $(r_1, \dots, r_{m_{max}})$.
- For each of the estimated rotation rates in step 1 check if it is in Ω.
  - If no such match is found, then assume it is the lowest harmonic and add the pair $(r_1, [1])$ to Ω.
  - If a rotation rate, r_k, is similar to a r_l such that $(r_l, [1, \dots, l])$ is in Ω, then update the element of Ω with $(r_l, [1, \dots, l, k])$. That is, add k to the observed harmonic numbers for the existing rotation rate.

In this manner, the set of possible rotation rates is built from the lowest numbered harmonic to the highest. The reason for this choice is the fact that the lower numbered harmonic components have the largest amplitudes and are thus the most likely to be observed. Furthermore, when starting from the center of the range cell, the lower harmonic numbers are most likely.

2.3.2.4 Filtering

The set of possible rotation rates often contain multiple false rotation rate predictions and require filtering. The filters used by CODAR during WTI mitigation thresholds include:

- Thresholding by the number of peaks 5 dB stronger than the average signal in the same Doppler bin
- Removing estimated rotation rates that don't fall within the operational rotation rates of the turbine.

The construction of Ω allowed rotation rates with a single pair of WTI peaks to be included in the set of possible rotation rates. However, if it is known that more than the first harmonic component should be observed, a threshold should be used to reduce false rotation rate estimations. Furthermore, there can be narrow bands of interference in the range-Doppler spectra that are symmetric to zero Doppler. To prevent banded interference from being processed as WTI, each of the peaks found is compared to the average signal in the Doppler bin containing the peak. The average is taken across all range bins. Comparing the signal strength of the suspected WTI peak to the average signal strength in the Doppler cell indicates when the peak is isolated in range and not a result of vertical interference. A range slice with the average at each Doppler bin is shown in Figure 14. For the 5 MHz system at Block Island, it was found that requiring at least two pairs of harmonic peaks with a signal 5 dB above the average in the Doppler cell produced the best results. The required number of harmonic pairs is specified in the mitigation configuration file.
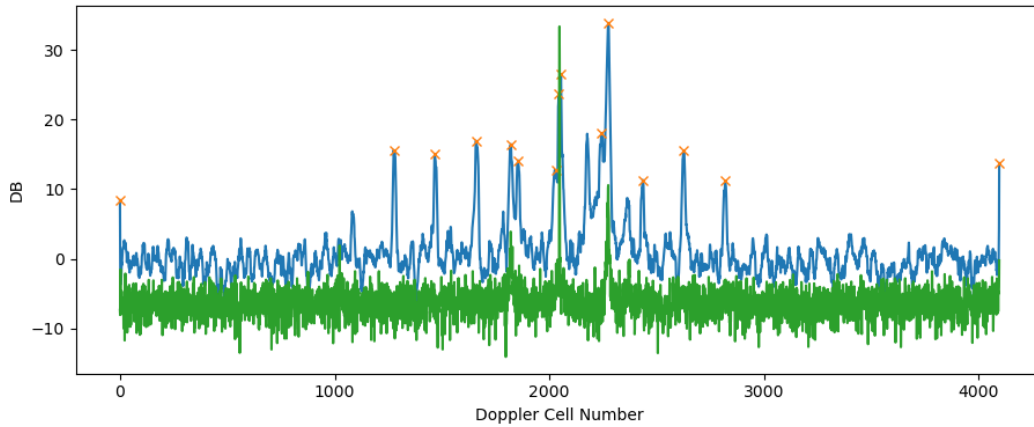
Figure 14: A range slice from a SeaSonde cross spectra containing WTI. The blue line shows the SNR of the range cell, the orange markers indicate WTI peaks found with the peak finding algorithm, and the green line shows the average SNR in the Doppler cell across all ranges.

It is also necessary to restrict the predicted rotation rates based on the possible rotation rates of the turbine in a wind farm. Knowing the minimum and maximum rotation rates possible allows the restriction of the estimated rotation rates and can be set in the configuration file

2.3.3 Forward Problem

Once the difficult task of estimating the rotation rates from the wind turbines is complete, equation (3) is used with the estimated rotation rates and their estimated variation to flag the Doppler cells that likely contain WTI. An example of a spectra flagged utilizing this method is shown in Figure 15.
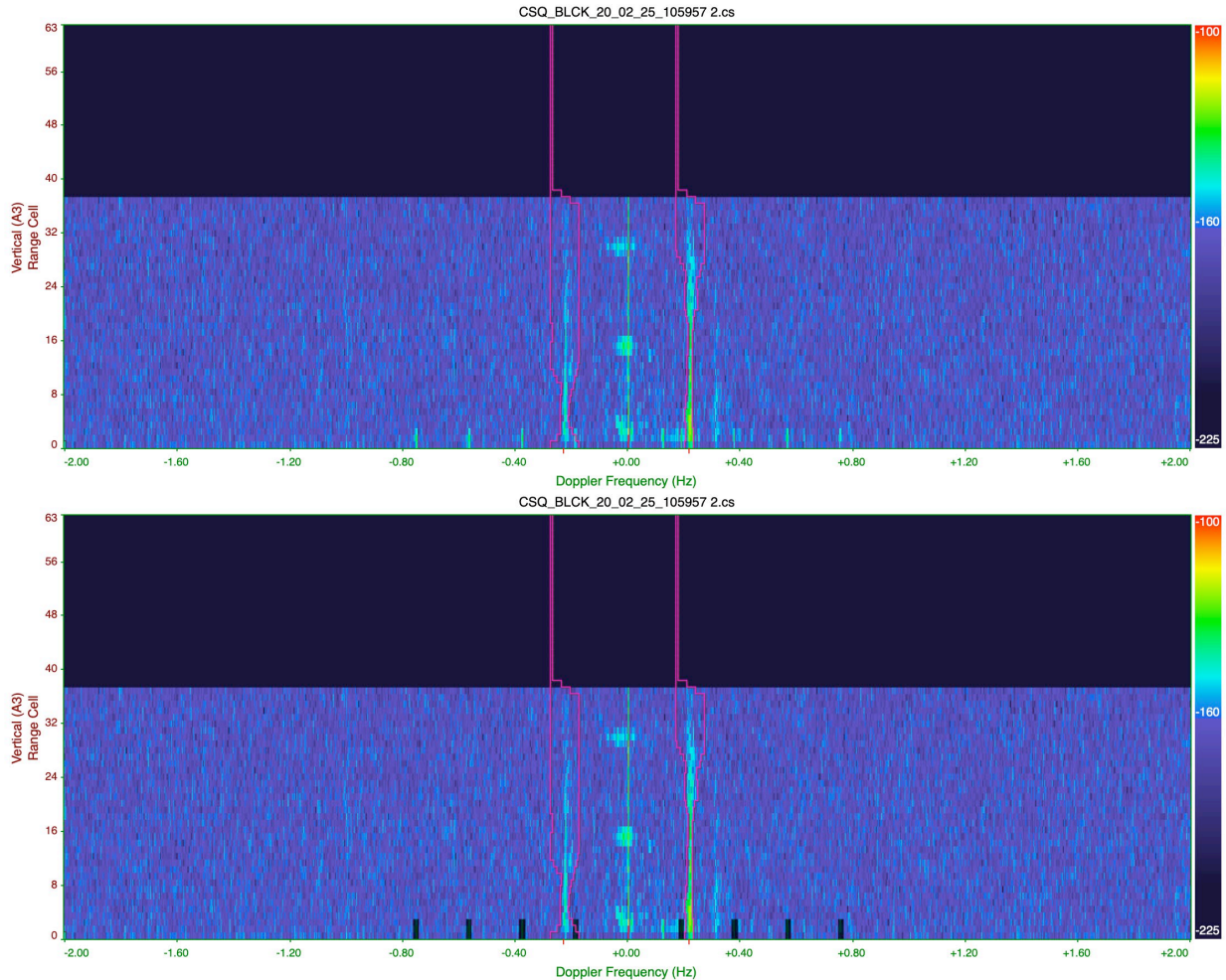
Figure 15: A range-Doppler spectra from BLCK with observed wind turbine interference in the first range cell (top). The same range-Doppler spectra from BLCK showing the flagged range-Doppler bins using the WTI mitigation method explained above (Bottom). The magenta lines indicate the boundaries of the first-order region.

2.4   Assessment

This section describes the data sets and tests used to assess the effectiveness of the mitigation method outlined above.

2.4.1   Datasets

A data set including SeaSonde range-Doppler spectra files paired with the rotation rates and yaw angles of the turbines at corresponding times is needed to assess mitigation. At Block Island, a time series spanning 2/22/2020 to 4/3/2020 of Doppler cross-spectra from the 5 MHz BLCK radar station (owned and operated by Rutgers University) was made available for mitigation testing. The radar was running with a sweep rate of 4 Hz during the collection time to prevent aliasing of the first three positive and negative harmonic peaks. Complementing the SeaSonde data, a time series of the rotation rates and yaw angles of each of the turbines was provided from each of the turbines' SCADA (Supervisory Control and Data Acquisition) systems. The data

were provided by the turbine operator, Ørsted, via BOEM. The relevant variables in the SCADA data include the rotation rates and the wind direction measured at each of the turbines. It was assumed that the nacelle of each of the turbines was always pointing directly into the wind. Assuming the turbines always face the wind, the yaw angle is estimated to be the direction from which the wind was blowing. However, the data did not include a reference bearing for the wind direction, and the data set needed to be calibrated before use. For details, see Appendix A. The combination of the radar and SCADA data mentioned above will be referred to as the field data below.

The simulation data set discussed in the simulation section was used in conjunction with the field data to test the capabilities of the mitigation method outlined above. The simulations provide the opportunity to test the mitigation software with a larger number of turbines in a single range cell to indicate the expected performance as more turbines are constructed in U.S. waters.

2.4.2 Mitigation Assessment

The test and measures used by CODAR to assess the mitigation of WTI include the percent reduction of the WTI in the Bragg and the percent of flagged range-Doppler bins in the first-order region that do not contain WTI. For testing purposes, the rotation rates from the SCADA systems are used with equation (3) to identify the range-Doppler bins containing WTI compared to those predicted by the mitigation software.

The percent reduction of the WTI in the Bragg is obtained as the percentage of range-Doppler bins identified with the SCADA data to have interference in the Bragg that were flagged using the mitigation software. Similarly, the percent of flagged range-Doppler bins in the first-order region that do not contain WTI is calculated as the percentage of flags from the mitigation software in the Bragg region that do not match flags in the Bragg region predicted by the rotation rates from the SCADA data.

3 Results

This chapter presents the results of the mitigation assessment only. First, the improvements from adjusting the radar's operational parameters are shown, followed by the evaluation of the software mitigation tool. The interpretation and implications of these results are given in the next chapter.

3.1 WTI Reduction from Reducing the Sweep Period

As shown in chapter two, reducing the sweep period reduces the WTI in the Bragg by reducing aliasing. To measure the reduction in interference in the Bragg region from changing the sweep period, equation (3) was used to identify all the rotation rates that would place any of the first four positive or negative WTI harmonic peaks in the Bragg region (corresponding to ±1 m/s) for a sweep rate of 1 Hz and 4 Hz. The rotation rates from the SCADA data were then used to find the total hours the wind turbine would place WTI in the Bragg during the field test for a radar operating with a sweep rate of 1 Hz and 4 Hz. Figure 16 shows a histogram of the rotation rates during the field test where the gray regions show the rotation rate intervals placing WTI in the

Bragg. The only meaningful statistic for assessing the improvements from adjusting the sweep rate is the percent reduction which is shown in Table 4. By preventing aliasing, the impact of WTI on the Bragg region is reduced by 77.9% on the 5 MHz SeaSonde at Block Island.
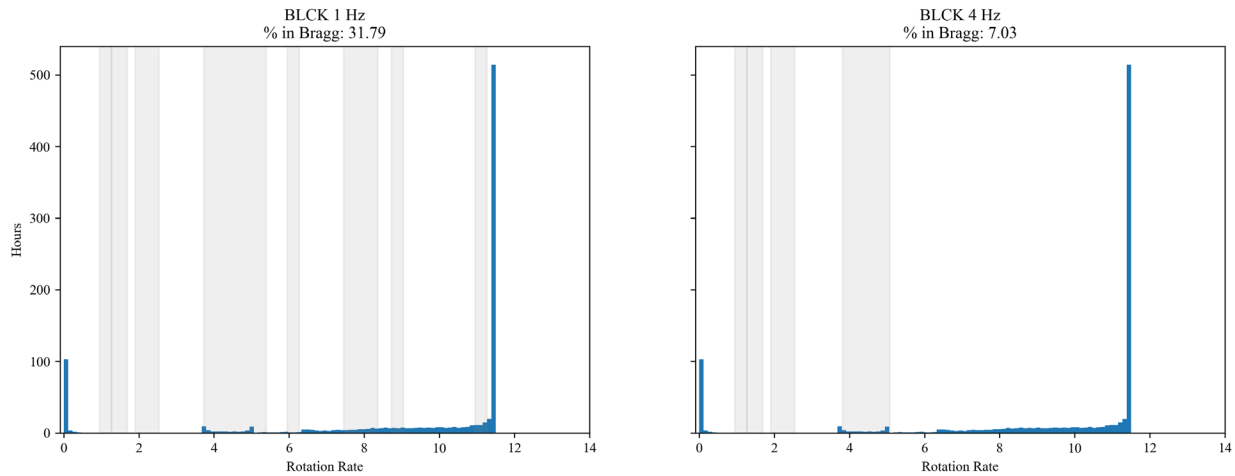
Figure 16: Histograms of rotation rates from turbines at Block Island from March 2020. The gray regions indicate rotation rates that place WTI in the Bragg when the 5 MHz radar has a sweep rate of 1 Hz (left) and 4 Hz (right).

3.2   WTI Reduction Through Software Mitigation

For the mitigation software assessment, the sweep rate of the radar was set to 4 Hz, so all reductions to the WTI should be considered additional improvements. The results from the evaluation of the mitigation software are shown in Table 4. For the simulations, the percent reduction of the WTI in the Bragg improved as the number of turbines increased. This is likely a result of flagging a higher percentage of the total Doppler cells in the Bragg region. Additionally, for all the simulation tests, the mitigation worked better when the maximum WTI peak was scaled to have the same SNR as the maximum signal in the Bragg.

For the assessment with the field data, the mitigation software reduced the impact of the WTI in the Bragg by 39%, in addition to the 78% reduction from the sweep period adjustment to 0.25 seconds. As a result, the sweep period adjustment and the mitigation software reduced the WTI in the Bragg region by 86%.

Table 4: Results from the WTI mitigation assessments. The *% Reduction* is the reduction of the WTI in the Bragg region, and the *% Error* is the percentage of flagged Doppler cells flagged that should not have been flagged.

	% Reduction	% Error
Sweep Period Reduction	77.9%	n/a
Software Mitigation Simulation 5 Turbines (-15 dB < Bragg)	14.8%	46.8%
Software Mitigation Simulation 15 Turbines (-15 dB < Bragg)	28.0%	23.1%
Software Mitigation Simulation 30 Turbines (-15 dB < Bragg)	44.0%	13.3%
Software Mitigation Simulation 5 Turbines (0 dB < Bragg)	44.3%	40.9%
Software Mitigation Simulation 15 Turbines (0 dB < Bragg)	57.0%	32.9%
Software Mitigation Simulation 30 Turbines (0 dB < Bragg)	73.0%	26.9%
Software Mitigation Field Data	38.8%	55.6%
Software Mitigation and Sweep Period Reduction	86.4%	n/a

4   Discussion

This chapter explores the results from the previous chapter. Most notably, the low percent improvement of the software mitigation solution. Additionally, the expected impact of the WTI left after mitigation on surface current measurement is discussed.

The Block Island wind farm turbines have a minimum rotation rate of 3.5 RPM and a maximum rotation rate of 11.5 RPM. Examining the histogram in Figure 16 we see that turbines spend the most time with a rotation rate of around 11.5 RPM. This means that if the 5 MHz SeaSonde at Block Island has a sweep period of 0.25 or lower, only the first WTI harmonic peak will be in the Bragg region and even then, only for rotation rates less than 5.2 RPM. It is challenging to solve the inverse problem when the first harmonic WTI peak is placed in the Bragg region as it is the strongest harmonic peak.

Furthermore, by examining the rotation rates in the SCADA data provided by Ørsted, it is found that the lower rotation rates are less stable (i.e., they vary over the 1024 second Doppler FFT period). Therefore, variation in the rotation rates leads to a spreading of the WTI harmonic peaks in Doppler and reduces their SNR. Thus, the inverse problem must be solved using the second harmonic WTI peak with a reduced SNR for rotation rates placing WTI in the Bragg region.
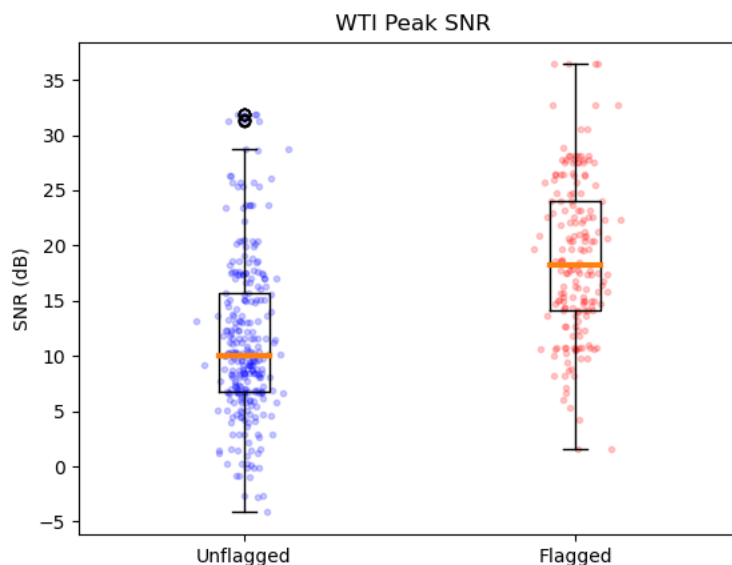
Figure 17: A box plot and scatter plot of the SNR values of the second harmonic WTI peak when the first harmonic interference peak is found in the Bragg region. The blue group on the left indicated the SNR values when the WTI mitigation software failed to flag the WTI in the Bragg region. In contrast, the red group on the right showed the SNR values at times the WTI mitigation software correctly flagged the WTI in the Bragg.

When looking closer at times the mitigation software was able to flag the WTI in the first-order region versus times it was unable to do so, we can see the SNR of the peaks is a likely cause. Figure 17 compares the SNR of the second harmonic WTI peak at times the first harmonic was placed in the Bragg. Times when the first harmonic WTI peak was flagged by the mitigation software are shown on the right in red, and times the software was unable to identify the first harmonic peak are shown on the left in blue. There is a decrease in the SNR of the second harmonic interference peak during times mitigation software failed to flag the WTI in the Bragg region. The reduction in the SNR is likely due to the width of the harmonic peaks caused by the variation in the rotation rate.

Since the times the WTI in the Bragg region corresponded to times the SNR of the WTI was lower, the impact of the WTI would be lessened as well. Furthermore, due to the transient nature of the rotation rates when the rotation rates are low, any radial current vector produced from the unflagged range-Doppler cell will have a minimal impact once it is averaged. The radial current vector observations are filtered and averaged together in half-hour increments.

5   Conclusion

The overall result of using the mitigation strategies outlined in this report has led to an estimated reduction of 86% of wind turbine interference in the first-order region of SeaSonde range-Doppler spectra collected from a 5 MHz radar at block Island during the month of March 2021. However, to assess the full impact of the wind turbines on ocean current observations and the

improvements due to mitigation comparisons with other instruments such as drifters will be necessary. This represents a significant step forward in the mitigation of WTI. Similar results are expected at other sites with identical wind turbines. However, if the size of the turbines increase resulting in a decrease in the optimal rotation rates, the WTI could more consistently mix with the Bragg echo and increase the impact. Larger turbine sizes could also affect the spacing of the turbines within the wind farms leading to a reduction in the number of turbines found in a range cell. The distance of the turbines from shore will affect the amplitude of the observable interference. Turbines that are placed further from the radar will have a reduced WTI but also be more difficult to identify and remove. Other shortcomings in the developed mitigation strategy include data loss due to flagging and elimination of range-Doppler cells with suspected WTI. Results indicate an increase in the loss of ocean observations as the number of turbines in a range cell increases if the turbines are not operating at the same rotation rates. This can likely be mitigated with the installation of additional SeaSondes to fill in the gaps caused by WTI.

6 Works Cited

Abascal, A. J., Sanchez, J., Chiri, H., Ferrer, M. I., Cárdenas, M., Gallego, A., Castanedo, S., Medina, R., Alonso-Martirena, A., & Berx, B. (2017). Operational oil spill trajectory modelling using HF radar currents: A northwest European continental shelf case study. *Marine pollution bulletin*, *119*(1), 336-350.

Colburn, R. J., Randolph, C. A., Drummond, C., Miles, M. W., Brody, F. C., McGillen, C. D., Krieger, A. S., & Jankowski, R. E. (2020). Radar Interference Analysis for Renewable Energy Facilities on the Atlantic Outer Continental Shelf. OCS Study, McLean. *Sterling, VA: US Department of the Interior, Bureau of Ocean Energy Management. OCS Study BOEM*.

Kirincich, A. (2016). Remote sensing of the surface wind field over the coastal ocean via direct calibration of HF radar backscatter power. *Journal of Atmospheric and Oceanic Technology*, *33*(7), 1377-1392.

Kirincich, A. R., Cahl, D., Emery, B., Kosro, M., Roarty, H., Trockel, D., Washburn, L., & Whelan, C. (2019). High Frequency Radar Wind Turbine Interference Community Working Group Report. In: Woods Hole Oceanographic Institution.

Lipa, B., Barrick, D., & Isaacson, J. (2016). Coastal Tsunami Warning with Deployed HF Radar Systems. *Tsunami*, 73.

Roarty, H., Kohut, J., Glenn, S., & Marcoos Principal, I. (2008). The Mid-Atlantic Regional Coastal Ocean Observing System: Serving Coast Guard and Fisheries Needs in the Mid-Atlantic Bight.

Roarty, H. J., Smith, M., Glenn, S. M., Barrick, D. E., Whelan, C., Page, E., Statscewich, H., & Weingartner, T. (2013). Expanding maritime domain awareness capabilities in the arctic: High Frequency radar vessel-tracking.

Teague, C. C., & Barrick, D. E. (2012). Estimation of wind turbine radar signature at 13.5 MHz. 2012 Oceans,

Trockel, D., Rodriguez-Alegre, I., Barrick, D., & Whelan, C. (2018). Impact Assessment and Mitigation of Offshore Wind Turbines on High Frequency Coastal Oceanographic Radar.

Sterling, VA: US Department of the Interior, Bureau of Ocean Energy Management. OCS Study BOEM, *53*, 49.

Wyatt, L., Robinson, A., & Howarth, M. (2011). Wind farm impacts on HF radar current and wave measurements in Liverpool Bay. OCEANS 2011 IEEE-Spain,

A Calibration

Before the SCADA (Supervisory Control and Data Acquisition) is used to assess the wind turbine interference mitigation, any discrepancies (i.e., time shifts or yaw angles) between the radar data and SCADA data for each turbine in the wind farm were removed. The SCADA data that was provided contained yaw and rotation rates for the five turbines in ten-minute increments. The radar provided a range-Doppler spectra every 1024 seconds. Since the two data sets were temporally miss-aligned, quadratic interpolation was used to interpolate the rotation rates and yaw angles to the center time of each of the cross-spectra. Using the interpolated rotation rates did not yield WTI peaks in the same locations in both the simulated spectra and the radar spectra. One possible explanation for the different locations of the WTI peaks is the difference in the reference times of the two data sets. To correct for this, the peak location error was measured using the difference in predicted location of the first two positive and negative harmonic peaks, $b_m^p(t)$, and the location observed in the radar cross-spectra, $b_m^r(t)$. The distance measure used is given by

$$d(\tau) = \frac{1}{4N} \sum_{t=0}^{N} \sum_{m=-2}^{2} \left| b_m^p(t) - b_m^r\big(t + b_i^r(t)\big) \right|.$$

Where τ is the time shift in seconds, m is the harmonic number, and N is the total number of SeaSonde range-Doppler files used for the comparison. The correct time shift was estimated by choosing the value of τ that minimized $d(\tau)$ over the interval $\tau \in [-200, 1100]$ seconds.
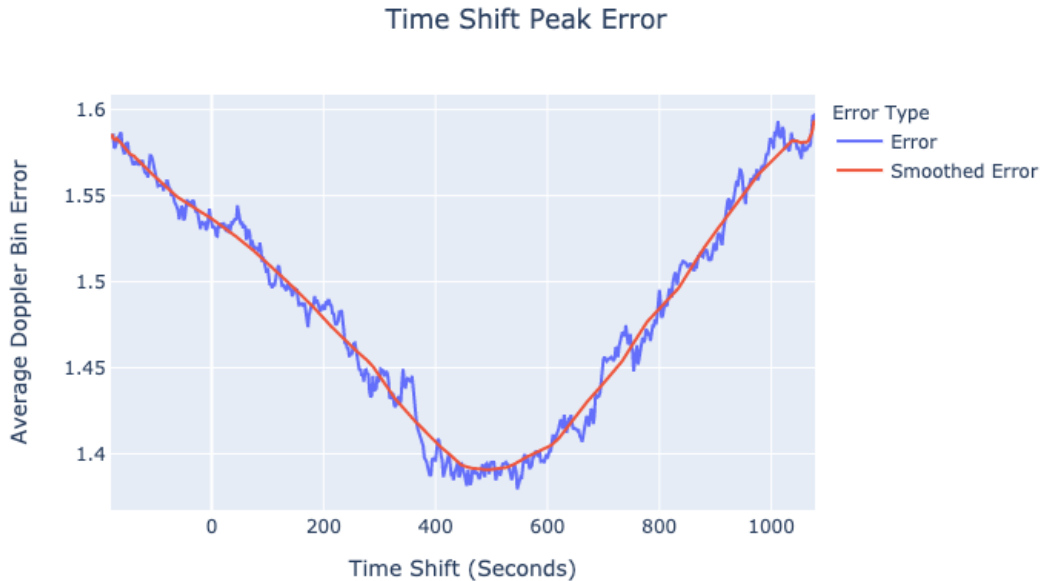
Figure 18: The average absolute error in WTI peak locations for time shifts of the SCADA data rotation rates.

Figure 18 shows a plot of the distance measure applied to the Block Island data set as the time was shifted between the two data sets. A minimum distance is achieved with a time shift of 497

seconds. Before the following calibration steps, the time shift of 497 seconds was applied to the SCADA Data.

Yaw Angle Time Series
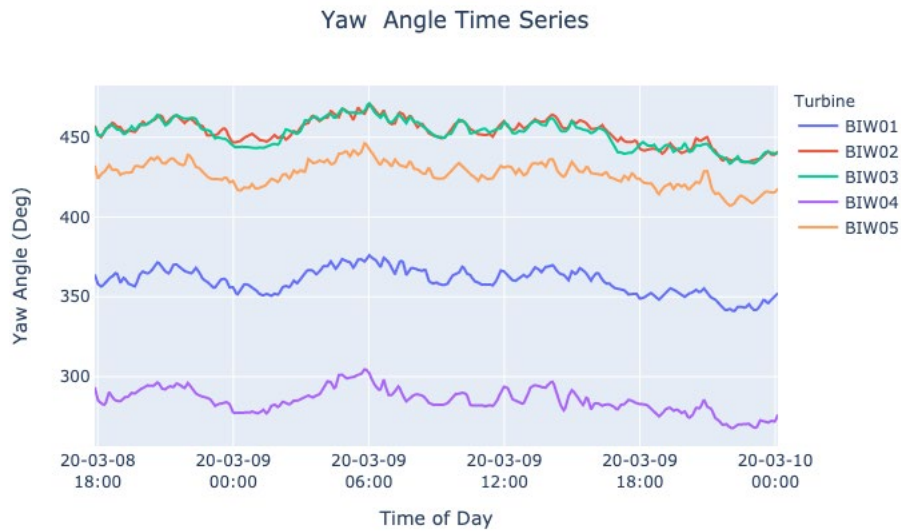
Figure 19: A plot of the time series of wind directions provided in the SCADA data. The strong correlation and consistent shift in the data indicate that the reference angle of each turbine is different and not measured as degrees clockwise from true north.

Once the time shift was correct, the yaw angles needed to be shifted as well. While the wind directions reported in the SCADA data were highly correlated, with a R^2 value no less than 0.9 between any two turbines, the reference angles of each of the turbines were different. In Figure 19, we plot the yaw angles, estimated from the wind direction, for each turbine. Figure 19 highlights the strong correlation between the yaw angles of the turbines, despite the 70° spread in yaw angles between the turbines.

We adjust for the ambiguity of the reference angle in the SCADA data using the least-squares method to align the yaw angles of the turbines with the BIW01 turbine. The results of aligning the yaw angles with BIW01 are shown in Figure 20.
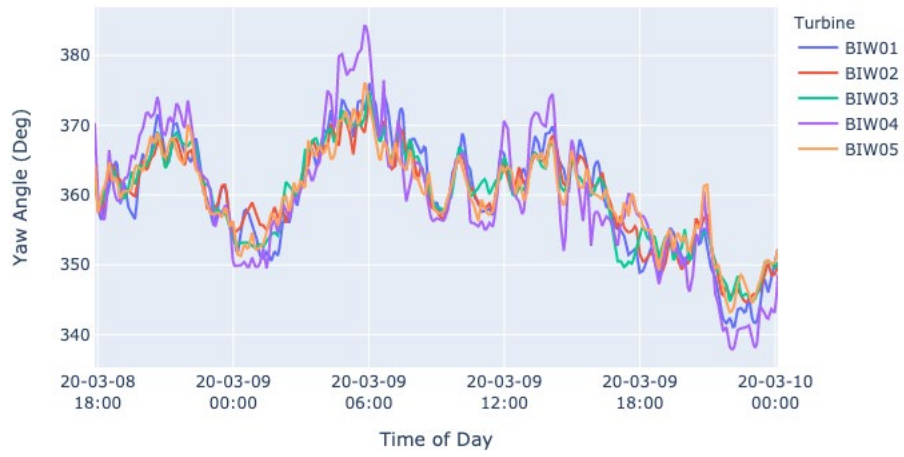
Figure 20: A plot of the time series of wind directions provided in the SCADA data after the yaw angles for each of the turbines are aligned with the BIW01 turbine.

U.S. Department of the Interior (DOI)
DOI protects and manages the Nation's natural resources and cultural heritage; provides scientific and other information about those resources; and honors the Nation's trust responsibilities or special commitments to American Indians, Alaska Natives, and affiliated island communities.

Bureau of Ocean Energy Management (BOEM)
BOEM's mission is to manage development of U.S. Outer Continental Shelf energy and mineral resources in an environmentally and economically responsible way.

BOEM Environmental Studies Program
The mission of the Environmental Studies Program is to provide the information needed to predict, assess, and manage impacts from offshore energy and marine mineral exploration, development, and production activities on human, marine, and coastal environments. The proposal, selection, research, review, collaboration, production, and dissemination of each of BOEM's Environmental Studies follows the DOI Code of Scientific and Scholarly Conduct, in support of a culture of scientific and professional integrity, as set out in the DOI Departmental Manual (305 DM 3).